

AL-TR-1991-0056

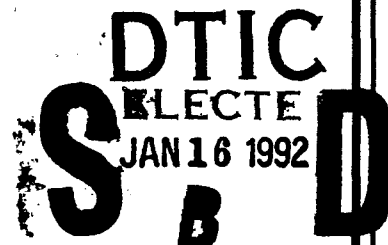
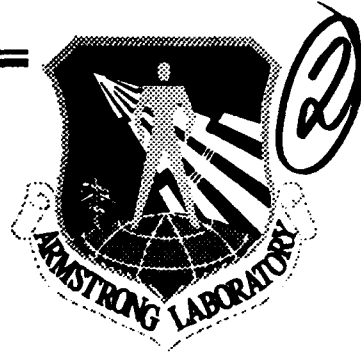
AD-A244 473



**MILLIMETER-WAVE EXPOSURE
SYSTEM AUGMENTATION**

Wesley W. Shelton

Bioengineering Center, CRB/0329
Georgia Institute of Technology
Atlanta, GA 30332



**OCCUPATIONAL AND ENVIRONMENTAL
HEALTH DIRECTORATE
Brooks Air Force Base, TX 78235-5000**

November 1991

Final Technical Report for Period June 1989 - June 1990

Approved for public release; distribution is unlimited.

92-01332



02 1 15 001

**AIR FORCE SYSTEMS COMMAND
BROOKS AIR FORCE BASE, TEXAS 78235-5000**

ARMSTRONG

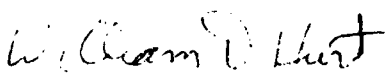
LABORATORY


NOTICES

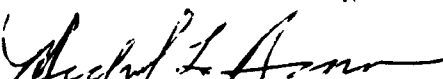
When Government drawings, specifications, or other data are used for any purpose other than in connection with a definitely Government-related procurement, the United States Government incurs no responsibility or any obligation whatsoever. The fact that the Government may have formulated or in any way supplied the said drawings, specifications, or other data, is not to be regarded by implication, or otherwise in any manner construed, as licensing the holder or any other person or corporation; or as conveying any rights or permission to manufacture, use, or sell any patented invention that may in any way be related thereto.

The Office of Public Affairs has reviewed this report, and it is releasable to the National Technical Information Service, where it will be available to the general public, including foreign nationals.

This report has been reviewed and is approved for publication.


WILLIAM D. HURT, M.S.
Project Scientist


DAVID N. ERWIN, Ph.D.
Chief, Radiofrequency Radiation Branch


MICHAEL L. BINION, Lt Col, USAF, BSC
Chief, Directed Energy Division

REPORT DOCUMENTATION PAGE			Form Approved OMB No 0704-0188	
<small>Public reporting burden for this collection of information is estimated to average 1 hour per response, including the time for reviewing instructions, searching existing data sources, gathering and maintaining the data needed, and completing and reviewing the collection of information. Send comments regarding this burden estimate or any other aspect of this collection of information, including suggestions for reducing this burden, to Washington Headquarters Services, Directorate for Information Operations and Reports, 1215 Jefferson Davis Highway, Suite 1204, Arlington, VA 22202-4302, and to the Office of Management and Budget, Paperwork Reduction Project (0704-0188), Washington, DC 20503.</small>				
1. AGENCY USE ONLY (Leave blank)		2. REPORT DATE November 1991	3. REPORT TYPE AND DATES COVERED Final June 1989 to June 1990	
4. TITLE AND SUBTITLE Millimeter-wave Exposure System Augmentation			5. FUNDING NUMBERS C - F33615-87-D-0626/0006 PE - 62202F PR - 7757 TA - 01 WU - 1G	
6. AUTHOR(S) Wesley W. Shelton				
7. PERFORMING ORGANIZATION NAME(S) AND ADDRESS(ES) Bioengineering Center, CRB/0329 Georgia Institute of Technology Atlanta, Georgia 30332 - 0001			8. PERFORMING ORGANIZATION REPORT NUMBER	
9. SPONSORING / MONITORING AGENCY NAME(S) AND ADDRESS(ES) Armstrong Laboratory Occupational and Environmental Health Directorate Brooks Air Force Base, TX 78235-5000			10. SPONSORING / MONITORING AGENCY REPORT NUMBER AL-TR-1991-0056	
11. SUPPLEMENTARY NOTES				
12a. DISTRIBUTION / AVAILABILITY STATEMENT Approved for public release; distribution is unlimited.			12b. DISTRIBUTION CODE	
13. ABSTRACT (Maximum 200 words) <p>Dielectric lenses, a pedestal, and a remote-controlled positioner were designed, constructed, delivered, and installed for the Armstrong Laboratory/OEDR millimeter-wave facility which consists of a 75-W 35-GHz transmitter, a 50-W 94.5-GHz transmitter and a millimeter-wave anechoic chamber. Gaussian optics was used in the lens design and concentric sets of grooves were used to optimize the transmission characteristic of the lenses by impedance matching. With the lenses, power densities on the order of 1 W/cm^2 can be produced for a spot with a 3-cm (1.18 in.) diameter. A pedestal system was designed and constructed which could support specimens and be millimeter-wave transparent. The remote-controlled positioner is capable of positioning a millimeter-wave field probe within a 1 m X 0.5 m X 0.5 m (3.28 ft X 1.69 ft X 1.69 ft) volume. The system is also capable of feeding back to a remote computer the position of the probe.</p>				
14. SUBJECT TERMS Millimeter-wave; Dielectric lenses; Remote-controlled positioner; Gaussian optics; Millimeter-wave chamber			15. NUMBER OF PAGES 60	
			16. PRICE CODE	
17. SECURITY CLASSIFICATION OF REPORT Unclassified	18. SECURITY CLASSIFICATION OF THIS PAGE Unclassified	19. SECURITY CLASSIFICATION OF ABSTRACT Unclassified	20. LIMITATION OF ABSTRACT UL	

TABLE OF CONTENTS

INTRODUCTION.....	1
DIELECTRIC LENSES.....	2
Design Concepts.....	2
Gaussian Optics.....	2
Dielectric Materials.....	5
Lens Design.....	6
Simulated Quarter-Wavelength Matching.....	8
Lens Mounting and Alignment.....	12
Lens Performance.....	15
PEDESTAL ASSEMBLY.....	16
Design Concepts.....	16
Materials.....	17
Final Pedestal Design.....	17
Pedestal Performance.....	24
OPEN-WAVEGUIDE FIELD PROBES.....	25
Design Concepts and Components.....	25
Probe Performance.....	26
REMOTE-CONTROLLED POSITIONER.....	28
Design Concepts.....	28
Positioner System Components.....	32
Mechanical Design.....	33

Positioner Performance.....	34
REFERENCES.....	38
APPENDIX: Photographs of Machined Surfaces.....	39

List of Figures

FIG.	
<u>NO.</u>	
1.	Geometry of the single biconvex lens Gaussian transmission system.....4
2.	Details of the grooving of a dielectric lens refracting surface.....10
3.	Entire positioning table with the 35-GHz lens and its placement relative to the antenna aperture.....13
4.	Schematic drawing of the lens positioner system.....14
5.	Styrofoam platform mounted on the pedestal system with the 35-GHz field probe positioned above the 2,000 cm ² surface.....18
6.	Schematic drawing of the Styrofoam column showing the component parts. The upper figure shows the mounting surface from the top, while the lower 2 figures present a sideview of the 2 parts of the column.....19
7.	Pedestal system upon completion of construction at the Georgia Tech Machine Shop.....21
8.	An end-view of the pedestal system upon completion of construction at the Georgia Tech Machine Shop.....22

9.	Schematic drawing of the pedestal system.....	23
10.	Plot of the HP 432B power meter output vs. the transmitter setting.....	29
11.	Plot of the HP 432B output vs. the Narda field probe at 35-GHz. Transmitter settings (mW) are given in the parentheses.....	30
12.	Close-up of the 35-GHz probe showing the waveguide, thermistor mount, wooden positioner arm, and the output cable.....	31
13.	The 3-axis positioning system from the front showing all 3 rails and the wooden arm extending from the vertical rail out over the pedestal.....	35
14.	The 3-axis positioner system from the rear looking out over the pedestal system.....	36
15.	The 3-axis positioner system showing the potentiometer and gear arrangement for positioning feedback.....	37
A-1.	Basic cylindrical block of Rexolite to be machined into the biconvex 35-GHz dielectric lens.....	39
A-2.	Another view of the Rexolite block of Figure A-1 following surface contouring.....	40
A-3.	Machining of one of the 35-GHz lens surfaces.....	41
A-4.	Completed contouring of the lens surface.....	42
A-5.	Another view of the lens surface of Figure A-4. Note the discarded Rexolite.....	43
A-6.	Template being used to control surface contouring during the machining of the lens shown in Figures A-4 and A-5.....	44
A-7.	Grooving of one of the 35-GHz dielectric lens surfaces.....	45
A-8.	Another view of the surface grooving process of Figure A-7..	46

A-9. Finished 35-GHz lens clearly showing the grooving.....	47
---	----

List of Tables

TABLE NO.

1. Computer-generated lens design and performance specifications.....	8
2. Dimensions used for grooving the dielectric lenses.....	11
3. Measurement data from the 35-GHz open-waveguide field probe test.....	28

PREFACE

This Final Report describes the results of research and development pertinent to U.S. Air Force Contract F33615-87-D-0626/0006, "Millimeter-Wave Exposure System Augmentation," for the Radiation Sciences Division of the U.S. Air Force School of Aerospace Medicine, Brooks AFB, TX. The work was performed by personnel in the Bioengineering Research Center at the Georgia Institute of Technology, Atlanta, GA. The contract is identified at Georgia Tech as B-03-AO6. Dr. Wesley W. Shelton served as the Project Director. Other Bioengineering Research Center staff who contributed to this effort are hereby acknowledged: Mr. Jim Toler, Mr. Tom Single, and Mr. David Banks. The excellent quality of craftsmanship and cooperativeness provided by the Georgia Tech Research Institute Machine Shop personnel, Mr. Carroll Garrett, Mr. Gene Dixon, Mr. Mike DeFranks, and Mr. George Bearce is gratefully acknowledged.

Accession For	
NTIS GRA&I	<input checked="checked" type="checkbox"/>
DTIC TAB	<input type="checkbox"/>
Unannounced	<input type="checkbox"/>
Justification	
By	
Distribution/	
Availability Codes	
Dist	Avail and/or Special
A-1	

MILLIMETER-WAVE EXPOSURE SYSTEM AUGMENTATION

INTRODUCTION

We describe herein the design and development of instrumentation and devices to meet the requirements specified by Delivery Order 0006 of USAF Contract F33615-87-D-0626 for the augmentation of the millimeter-wave system at the USAF School of Aerospace Medicine (USAFSAM) (now Armstrong Laboratory), Brooks AFB, TX. This facility, created for the study of millimeter-wave bioeffects, consists of (1) a 75-W, 35-GHz transmitting system, (2) a 50-W, 94.5-GHz transmitting system, and (3) a temperature-controlled, millimeter-wave anechoic exposure chamber. The 2 transmitter systems are contained within the same rack external to the chamber. The millimeter-wave radiation (MWR) is emitted by either a 35-GHz or a 94.5-GHz corrugated conical horn antenna, since the transmitting systems cannot function simultaneously. With the original configuration, the maximum theoretical power densities at a boresight distance of 3 m (9.84 ft) (within the quiet zone) were 24 and 10 mW/cm² for 35 GHz and 94.5 GHz, respectively.

Thus, as originally configured, the system was inadequate for studying high incident power density (on the order of 1,000 mW/cm²) MWR bioeffects. The system also lacked a means of dosimetry, or power density measurement, crucial to bioeffects research.

Our aim was to augment the original exposure system to generate intense radiation and provide for radiation dosimetry. The task specified development and delivery of:

- (a) dielectric lenses for focusing the millimeter-wave beam, and thus creating high power densities,
- (b) two millimeter-wave-transparent pedestals for the support of experimental and dosimetric hardware in the exposure volume, and
- (c) a remote-controlled millimeter-wave probe for 3-dimensional dosimetry.

DIELECTRIC LENSES

Design Concepts

Dielectric lenses were required to achieve the goal of increasing the power densities above those produced by uncorrected 35-GHz and 94.5-GHz corrugated conical horn antennas already in place in the millimeter-wave exposure chamber at USAFSAM. The power densities reported by USAFSAM personnel were 24 mW/cm² for the 35-GHz antenna and 10 mW/cm² for the 94.5-GHz antenna. The desired level for each frequency was on the order of 1 W/cm² at a distance of 3 m (3.28 ft) from the horn apertures. More specifically, 18% of the transmitted power was to fall within a 3 cm (1.18 in.) diameter spot at 3 m (9.84 ft) along boresight, while 98% was to fall within a 30 cm (11.81 in.) diameter spot at that point.

Initially, effort was spent investigating the feasibility of aperture-mounted planoconvex and meniscus lens (1,2) because of their relative simplicity with regard to mounting. Lengthy and complex analysis failed to show that these would produce the desired power densities even under ideal circumstances of precisely known phase centers and exactly formed interior dimensions of the 2 horns. Imperfections in lens and horn construction often produce "ringing" (resulting from reflections) which can be conveniently reduced by tilting the dielectric lens slightly around the elevation-angle axis, thereby diverting the reflected energy away from the horn aperture. In the case of fixed, aperture-mounted lenses, lens-tilting cannot be performed; therefore, non-aperture-mounted Gaussian lenses were selected.

Gaussian Optics

Gaussian optics techniques become applicable at millimeter wavelengths under the more appropriate description of "quasi-optical" techniques (3,4,5,6). These techniques apply when the radiated beams can be assumed to possess amplitude distributions of Gaussian form which are retained as the beam propagates and broadens (due to diffraction). Most high-performance feedhorns, such

as the corrugated conical horns used in the USAFSAM exposure chamber, have radiation patterns which are very nearly Gaussian (3). The mathematical expressions are well-developed and are relatively easy to use.

The application of Gaussian optics to lens design begins by locating the phase center of the horn antenna of interest because the "originating" beam waist is placed there. The millimeter-wave corrugated conical horn antennas of interest in this project were electroformed according to specifications by another contractor and that information, as well as any testing or analysis pertaining to the phase centers, was unavailable for this project. Therefore, the 2 antennas were shipped to Georgia Tech for measurement of gross dimensions (aperture radii, flare length, etc.) in order to estimate the phase center locations (3,7). Using 3 analytical methods, the phase centers for the 35-GHz and 94.5-GHz antennas were estimated to be 14.96 cm (5.89 in.) and 4.80 cm (1.89 in.), respectively, behind the aperture planes. The time (including labor and facilities scheduling) and cost of performing exacting field measurements of the phase centers was not considered necessary for the purposes of this project since tolerances to compensate for phase center uncertainty could be included in the lens design.

Figure 1 depicts the geometry applicable to a system using a single biconvex lens between the source and the target, and using Gaussian optics for design. The beam waist, or minimum cross-sectional area, of the Gaussian beam is placed at the estimated location of the horn antenna. From there, the beam expands in cross section according to this expression for the beam radius, which is the radius at which the Gaussian-distributed amplitude falls to 1/e of its peak value at the beam center

$$w(z) = w_0 \left[1 + \left(\frac{\lambda z}{\pi w_0^2} \right)^2 \right], \quad (1)$$

where $w(z)$ = is the beam radius as a function of the
distance from the beam waist,
 z = the distance from the beam waist along boresight,

λ = the free space wavelength, and
 w_0 = the beam waist radius.

The beam spherical wavefront is given as

$$R(z) = z \left[1 + \left(\frac{\pi w_0^2}{\lambda z} \right)^2 \right], \quad (2)$$

which describes the radius of curvature as infinite (plane wave) at the beam waist and as a decreasing function of distance from the beam waist. At a distance z from the beam waist, a lens can be centered on boresight and oriented perpendicular to it in order to transform the beam without altering the amplitude. This transformation is accomplished by inducing a phase shift across the lens and, thereby, changing the radius of curvature to create another beam waist on the output side of the lens. If precautions are taken to clear all obstructions from a coaxial (with boresight) cylindrical volume with a radius equal to approximately twice the largest beam

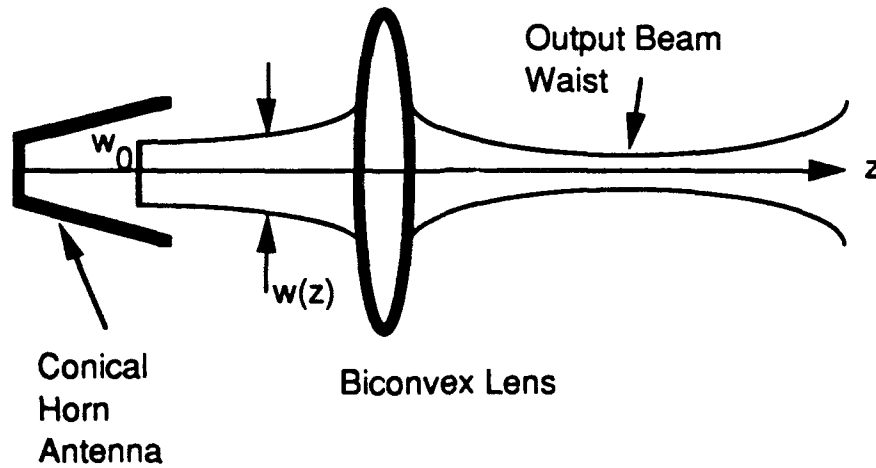


Figure 1. Geometry of the single biconvex lens Gaussian transmission system.

radius encountered along the propagation pathway, then negligible beam truncation can be assumed (5). With this condition, the fraction of power within a radius r_0 of the beam center can be computed according to the expression

$$f(r < r_0) = 1 - \exp\left(\frac{-2r_0^2}{w^2}\right). \quad (3)$$

Important lens design considerations include type (e.g., biconvex), radius, focal length, surface curvature, edge taper, thickness, permittivity, high power tolerance, hardness, opacity, and machinability. A number of trade-offs are encountered which address a balance among such factors as cost, size, lossy, etc. Cost must be considered in the purchase price of the raw dielectric material, in machining materials which might possess too high a degree of hardness, and in machining lenses of complex geometries. Although a large lens radius might be desirable, constraints can be encountered with respect to thickness (and hence, focusing performance) because of the sheer weight of the lens. Large, heavy lenses become unwieldy and difficult to manage, especially in the project at hand where the strength of metallic mounting and manipulating equipment has been sacrificed for weaker but more millimeter-wave transparent wooden components. On the other hand, achieving greater focusing power by designing thicker lenses incurs the penalty of greater attenuation of energy because of the longer transit paths through the dielectric. These considerations affect the overall system design because the positioning of the lenses with respect to the apertures is a function of lens properties.

Dielectric Materials

A number of dielectric materials for lens construction were investigated. Initially, TPX (poly-4-methylpentene-1) was chosen for lens construction based on literature reviews and discussions with other engineers experienced in millimeter-wave and submillimeter-wave design (8,9,10). TPX was determined to be the optimal dielectric with regard to low-losses, hardness, machinability, power-handling capability, cost, and optical transparency (which greatly facilitates optical alignment). We found that TPX was no longer available in the sizes needed for the lenses

to be constructed for this project, at least at reasonable cost. Attention was directed to Rexolite 1422 (a cross-linked polymer) (9) which possessed properties not too dissimilar to TPX and which appeared to find equal popularity among millimeter-wave and sub-millimeter-wave lens designers. For instance, the dielectric constant of Rexolite 1422 is approximately 2.54 in comparison to 2.24 for TPX, and both have a loss tangent on the order of 0.001 at the frequencies of interest. Rexolite is translucent except when its surface is moistened with mineral spirits whereupon a considerable improvement in transparency is achieved. The latter measure is too messy to warrant its use in alignment and requires lens surface cleaning, including the grooves in the surface, before proceeding with experimentation. Other products such as Teflon and high density polyethylene were evaluated in the early stages of this project and rejected based on reports of their poor performance (warping in the case of Teflon) under high-power conditions.

Rexolite 1422 was readily available from its manufacturer (C-LEC Plastics, Inc., Beverly, NJ) in several sizes. A 60.96 cm x 60.96 cm x 5.08 cm (24 in. x 24 in. x 2 in.) block was purchased for this project. The 2 nearest size options would force construction of lenses either too small or too large in diameter. The block constrained the maximum diameter for 2 equal-sized lenses to 35.36 cm (14 in.).

Lens Design

Biconvex lenses for both the 35-GHz and 94.5-GHz horns were selected for their simplicity in design and machining. A spreadsheet computer program was used to derive lens design specifications after several initial issues were settled.

The decision to use only 1 lens in the beam propagation path made it desirable to place the lens as far along boresight from the aperture as possible and still have the lens radius somewhat greater than the beam radius at that location. Each lens had a 16.31 cm (6.42 in.) radius and a 1.47 cm (0.58 in.) flange. Ideally, from a Gaussian optics standpoint, it would be desirable to have the lens radius at least 1.5 times the beam radius. Furthermore, the geometry of the lens frames and mounting table had to be considered since they would set the minimum distance from the apertures at which the

lenses could be placed. The size and weight of the lenses dictated the frame dimensions (116.13 cm² or 18 in.²) and the dimensions of the mounting table (upper surface was 193.55 cm² or 30 in.²) upon which the lens and frame would be mounted, to ensure durability and stability. The vertical axes of the lenses were at the center of the table surface and this placed the plane of the lenses approximately 38.1 cm (15 in.) from the rear of the table. Since the antennas were wall-mounted at an angle of approximately 16 degrees (from the wall normal) toward the chamber center and, since the range adjustment tracks in the table had to be aligned approximately along a line extending from the bisecting point between the apertures to the 3 m (9.84 ft) exposure point, the table itself had to be angled at approximately 16 degrees as well and would not be flush with the wall. Calculations showed that this arrangement would place the plane of the frame at a minimum of 50.8 cm (20 in.) from the apertures along boresight. This distance provided sufficient space to comfortably adjust the lenses during alignment. Demands placed on the lenses from the standpoint of focusing, power handling, and surface curvature would be reduced with increasing distance from the apertures. Additionally, the thickness of each lens surface would be reduced and this would translate into lower losses due to attenuation in the lenses. Reduced lens thickness also meant a flatter surface and this would become advantageous with regard to the assumptions made for the simulated quarter-wavelength matching addressed in the next section.

A computer program was used to optimize the lens design, given the location of the antenna phase center, desired output beam waist radius and location, and the lens radius. The lens design parameters yielded by the program are given in Table 1. The specifications regarding lens geometry were processed through a computer-aided design program to generate another set of specifications which, in turn, were used to control the lens machining instrumentation at the Georgia Tech Research Institute machine shop. Steel templates were machined to the specified contours for each of the 4 surfaces and were used to control the cutting of the lenses. Each biconvex lens was constructed by machining 1 surface to completion and then turning the disk over to machine the other, in contrast to the process of constructing 2 planoconvex lens and then attaching them at their planar surfaces to achieve a single biconvex lens.

**TABLE 1. COMPUTER-GENERATED LENS DESIGN AND
PERFORMANCE SPECIFICATIONS**

Input Lens	35 GHz	94.5 GHz
Distances (cm):		
aperture to output waist	300.01	276.36
aperture to phase center	4.75	10.97
phase center to input lens	90.00	90.00
Input beam waist (cm)	0.85	0.74
Beam radius at lens (cm)	13.34	12.61
Taper at lens edge (dB)	-12.97	-14.51
Lens focal length (cm)	91.78	90.30
Lens thickness (cm)	2.34	2.36
Output Lens		
Distance to output waist (cm)	215.25	187.72
Output beam waist (cm)	1.50	4.70
Focal Length (cm)	245.76	187.72
Lens Thickness (cm)	0.90	1.17
Power Density (W/cm ²)	1.86	5.90

Simulated Quarter-Wavelength Matching

Electromagnetic energy incident upon any surface with a permittivity other than unity will experience reflection to a degree dependent upon the permittivity value, the angle of incidence, and the polarization of the incident energy (11). An effective measure to

counter this phenomenon is to apply to the surface a coating of another dielectric possessing a permittivity which is the geometric mean of the interface permittivities (the incidence medium is usually taken to be air or free space). The thickness of such a coating would ideally be one-quarter of the wavelength of the energy in the impedance matching medium for normal incidence. For the hyperboloidal surfaces of the lenses used in this project, it could be shown that this depth is dependent upon the angle of incidence according to the expression

$$d = \frac{\lambda_g}{4}, \quad (4)$$

where:

$$\lambda_g = \frac{\lambda_0}{\sqrt{\epsilon_0 - \sin^2(\theta_i)}}, \quad (5)$$

where ϵ_0 = permittivity of matching section and

θ_i = angle of incident wave relative to surface normal.

The required dielectric constant can also be shown to be

$$\epsilon_0 = \sin^2(\theta_i) + \cos(\theta_i) \sqrt{\epsilon - \sin^2(\theta_i)}, \quad (6)$$

where ϵ = permittivity of the lens dielectric,

which means that it, too, is a function of the incidence angle; therefore, the coating cannot be homogeneous over the surface. Another concern with dielectric coatings is their susceptibility to abrasions and changing environmental conditions over long periods.

A more practical way of achieving reflection reduction is that of machining well-specified concentric sets of grooves directly into the lens surfaces (11). A cross-sectional view of a grooved lens is given in Figure 2. By controlling the width of the grooves, proper

amounts of the lens dielectric can be removed to yield an effective dielectric constant of any value desired. Thus, by properly choosing the ratio of slot thickness, $2t$, to slot spacing, D , the dielectric constant of the grooved layer can be varied over the lens surface to account for changes in the angle of incidence.

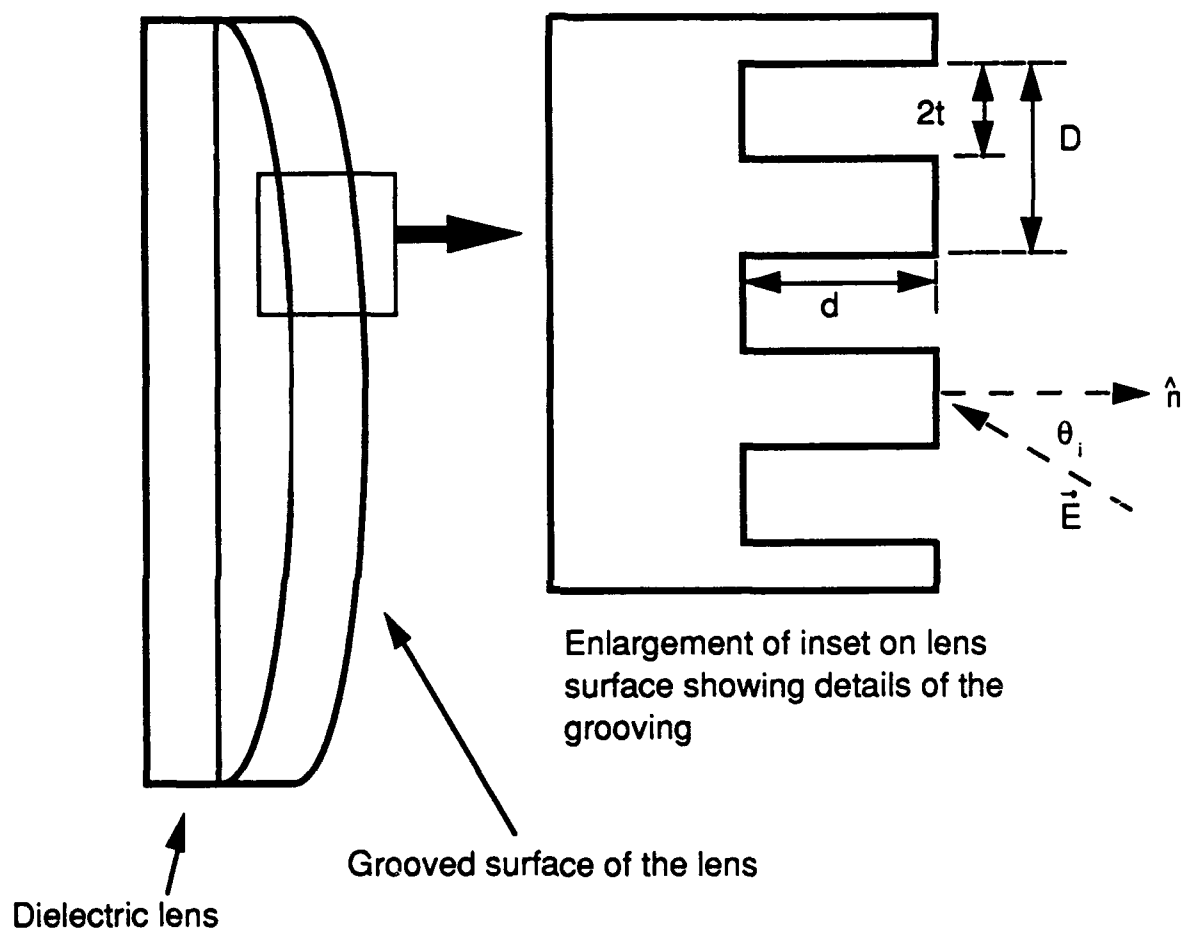


Figure 2. Details of the grooving of a dielectric lens refracting surface.

To reduce the number of slots, large spacings, D , are appealing. However, to avoid higher-order grating modes in the lens, D must be limited according to the expression

$$D < \frac{\lambda_0}{\sqrt{\epsilon + \sin^2(\theta_i)}} \quad (7)$$

Impedance matching measures are warranted in view of the lens permittivity of 2.54 and the desire to get as much of the available power to the 3 m (9.84 ft) point as possible in order to meet the 1 W/cm² goal. Surface grooving was the most practical way of approximating quarter-wavelength matching, and specifications for grooving both the 35-GHz and 94.5-GHz lenses were calculated.

The groove parameters, slot thickness, spacing, and slot depth can be ideally specified. Ideally, the slots (or grooves) are to be normal to the local surface into which they are cut. The outermost slot in the surface of a 16.30 cm (6.42 in.) radius lens located 90 cm (35.43 in.) along boresight from the phase center would receive energy at an incidence angle on the order of 26 degrees for either of the input lenses, and this is the maximum incidence angle to be expected. We found that the process of machining grooves specified even close to theoretical guidelines would be taxing to most machining operations and would clearly be prohibitively expensive. By placing the lens as far away from the apertures as possible (see last section), the lens surface curvature was reduced to a minimum. We decided that the degree of flatness achieved, especially at the center region of the surface, was sufficient to support the assumption of total flatness; therefore, the grooving parameters for normal incidence were computed and applied across the entire surface. The dimensions used for grooving the dielectric lenses are given in Table 2.

TABLE 2. DIMENSIONS USED FOR GROOVING THE DIELECTRIC LENSES

Dimension (cm)	35-GHz Lens	94.5-GHz Lens
Groove depth	0.2144	0.0792
Groove period	0.3429	0.1270
Groove width	0.1544	0.0572

Lens Mounting and Alignment

Figure 3 is a photograph of the positioning of the pedestal assembly and 35-GHz lens mounting table with respect to the horn antennas in the anechoic chamber. Figure 4 is a schematic of the lens positioning table.

Frames for each of the lenses consisted of pairs of 45.72 cm (18 in.) squares of particle board with circular holes machined into the centers. The hole diameters were approximately 34.29 cm (13.5 in.) on the outside surfaces of the 4 squares. On the inner surfaces of each square, the hole diameter was increased to 35.56 cm (14 in.) and cut to a depth of approximately 0.635 cm (0.25 in.) into the square. The inner surfaces of each pair were then pressed together around the circumferential flanges of the lenses, achieving a snug fit. The inner surfaces were glued beforehand to ensure a secure hold on the lens. Wooden pegs extended horizontally outward from the frames and fit into the yoke of the positioning table. This arrangement made it possible to easily interchange the lenses. The yoke was mounted atop the cylindrical wooden shaft used for lens height adjustment. The design was such that the axes of the (collinear) wooden pegs and the cylindrical vertical shaft intersected at approximately the geometric center of the lens mass. Once the height of the lens was adjusted to position its center in alignment with boresight, elevation angle adjustment (accomplished by rotation of the frame around the wooden pegs axis) and azimuth angle adjustment (accomplished by rotation of the frame around the axis of the vertical shaft) could be performed independently without perturbing the settings of each other. Once elevation angle was established, a wooden peg could be inserted into a slot between one of the pegs and the yoke to secure the angle setting. Since the height adjustment would be accomplished early in the alignment process, a reference mark could be placed on the shaft and azimuth rotation performed. Once the azimuth angle was selected, another wooden peg could be inserted into the base of the shaft assembly to secure both azimuth angle and height. After completing these measurements, range adjustment could be performed by moving the base of the shaft

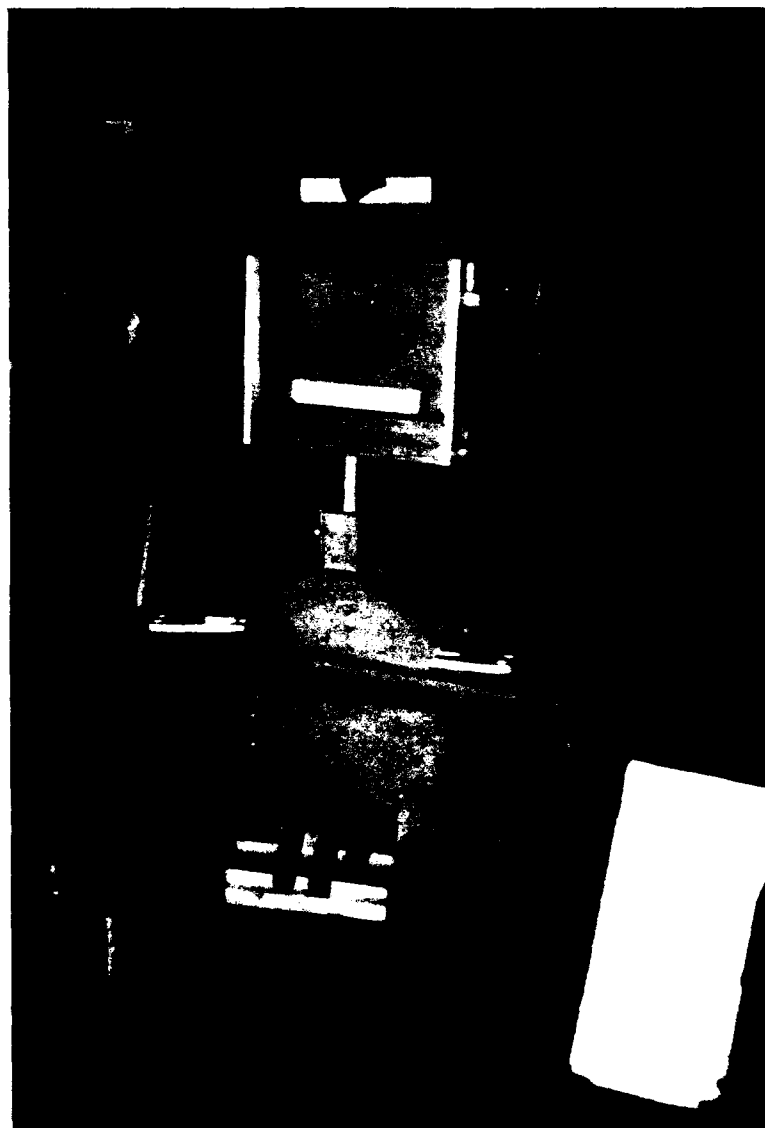


Figure 3. Entire positioning table with the 35-GHz lens and its placement relative to the antenna aperture.

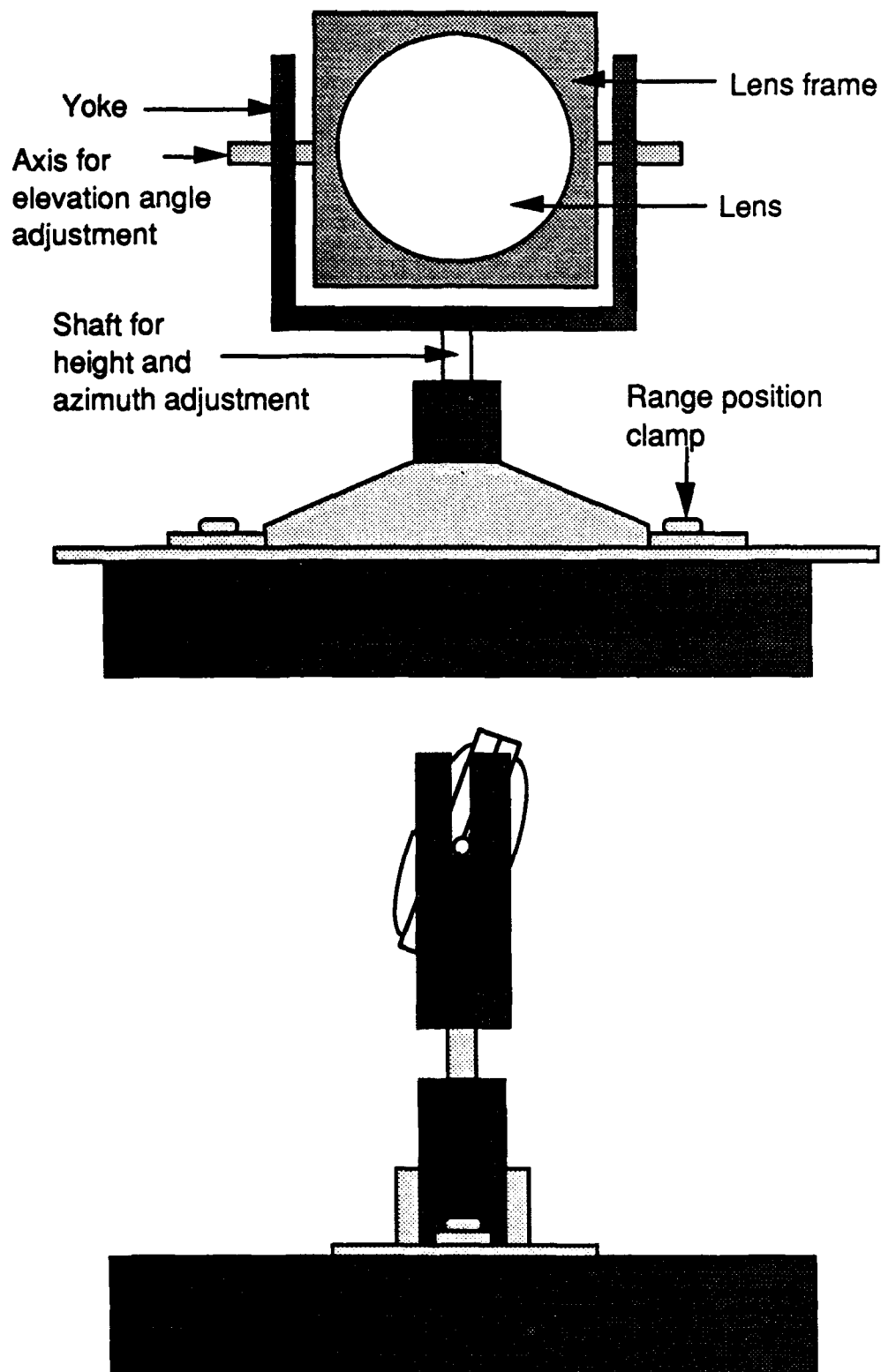


Figure 4. Schematic drawing of the lens positioner system.

assembly along boresight and locking it in place with the range position clamps. These alignment and adjustment procedures could be performed for either lens by first sliding the base of the shaft assembly sideways to a starting position in front of the antenna of interest and then placing the appropriate lens into the yoke. The lens, lens frame, and vertical shaft assembly sat upon a heavy 91.44 cm (36 in.) square table placed in front of the antennas. The table itself does not require movement during the alignment and adjustment procedures, and is heavy enough to provide a very stable platform for the lenses. The lens positioning system was constructed entirely of particle board and wood to achieve the maximum transparency to millimeter-wave energy.

Lens Performance

In June 1990, the lens mounting table and the 35-GHz lens were installed in the anechoic chamber at USAFSAM/RZP (now Armstrong Laboratory/OEDR). Alignment and testing of the lens at this time was performed within the limits of the Narda field monitors used to perform the basic dosimetry. A Helium-Neon laser (Class II) was mounted on the Styrofoam specimen mount of the pedestal and the height of the laser adjusted until the beam was centered down the throat of the 35-GHz antenna. This effort established the line-of-sight to the center of the Styrofoam surface. Both the laser and the Styrofoam surface were checked with levelers to ensure that they were truly level and, therefore, producing a horizontal beam. The lens was displaced off to the side during this portion of the alignment since it was translucent and obscured the laser beam. After line-of-sight (boresight) was established, the lens was moved into place and adjusted in height until the laser beam impinged upon its center. A leveler was used to adjust the lens frame until vertical alignment was achieved (zero elevation angle) and then adjusted by eye (estimated) for zero azimuth angle. The elevation of the laser beam above the plane of the Styrofoam mount surface was measured and used in establishing the zero (reference) position of the pedestal height with respect to line-of-sight. The laser was then removed and a calibrated Narda monitor placed on the Styrofoam mount. Successive adjustments in lens position (with transmitter power off during adjustment activities) were made along line-of-sight until a peak reading on the Narda monitor at the 3 m (9.84 ft) point was recorded. Additional adjustments in azimuth were then made until the Narda monitor peaked with the transmitter set at the

lowest power setting. Based on the speed at which the Narda peaked, we estimated that the system could most likely achieve the 1 W/cm² power density desired. More exacting dosimetry will be performed with the installation of the 3-dimensional positioner system and the open-waveguide field probes. Researchers from the University of Texas performing experiments with this system used an interesting technique to "visualize" the Gaussian beam cross-section: by suspending a slab of liver normal to boresight at the 3 m (9.84 ft) point, a round spot was burned into the liver. They found the spot (peak field) to be approximately 5.08 cm (2 in.) off to one side of boresight, and revealed the accuracy with which the lenses could be aligned through even the simple measures used for this preliminary alignment. The spot offset was compensated by moving the exposure setup to where the spot was located; the option of adjusting the lens in azimuth to move the spot itself was not exercised since the researchers were not familiar with the adjustment procedures at that time.

In September 1990, the positioner and open-waveguide field probes were delivered to USAFSAM/RZP and were used in October 1990, to map fields and more accurately determine the location of the peak field.

PEDESTAL ASSEMBLY

Design Concepts

This project undertook the design and construction of a pedestal system which would be capable of positioning and supporting 20 kg of weight anywhere along 50 cm (19.68 in.) of vertical travel in the anechoic chamber. Ideally, it would also be transparent to millimeter-wave energy. The original concept proposed 2 pedestals: (1) one with a surface area of 400 cm² and capable of supporting 4 kg (8.10 lbs) and (2) the other with a surface area of 2,000 cm² (310 in²) and capable of supporting 20 kg (40.49 lbs). However, we found that both requirements could be met with a single, 2-part structure: (1) an inner cylindrical column with an upper circular surface area of 400 cm² (62 in²) and (2) a larger octagonal column, crowned with a circular upper surface, hollowed-

out cylindrically along its axis to permit a snug fit over the inner column and create a combined upper surface area of 2,000 cm².

Materials

Materials used for the pedestal system had to balance the need for strength against the requirement for a high degree of millimeter-wave transparency. Styrofoam met the design goals for that portion of the pedestal system responsible for supporting prescribed specimen weights with the appropriate surface areas and offered the greatest practical degree of millimeter-wave transparency. However, the materials did not provide the mechanical strength needed in pedestal components which were to manipulate the specimen loads in a controlled fashion through 50 cm (19.69 in.) of vertical travel. For the latter pedestal components, wood appeared to be the optimal material with regard to strength and transparency. In particular, a high-grade marine plywood was selected for its lower vulnerability to humidity. Since some of the wooden components of the pedestal would be sliding against each other, considerable static and dynamic friction was expected, especially when the heavier experimental loads (20 kg or 40.49 lbs) were used. Additionally, the weight of the wooden components themselves would contribute to the frictional burden. To reduce the friction, strips of nylon were sparingly applied to those surfaces where friction would occur. Wooden dowels and wood glue were used to fasten all components. Marine plywood was used for the pedestal parts where any potential distortion due to humidity needed to be minimized. However, it was more practical to use other types of wood for a few other minor parts where distortion was not a concern.

Final Pedestal Design

The final pedestal design consisted of a Styrofoam platform, upon which the specimen would be mounted, and a wooden elevator system for moving the Styrofoam platform vertically through the field. The Styrofoam platform is shown in Figure 5 atop the wooden elevator system, and is schematically shown in Figure 6. The inner cylindrical component consisted of a circular base (17.78 cm or 7 in. radius and 21.16 cm or 8.33 in. height) upon which a cylindrical



Figure 5. Styrofoam platform mounted on the pedestal system with the 35-GHz field probe positioned above the 2,000 cm² surface.

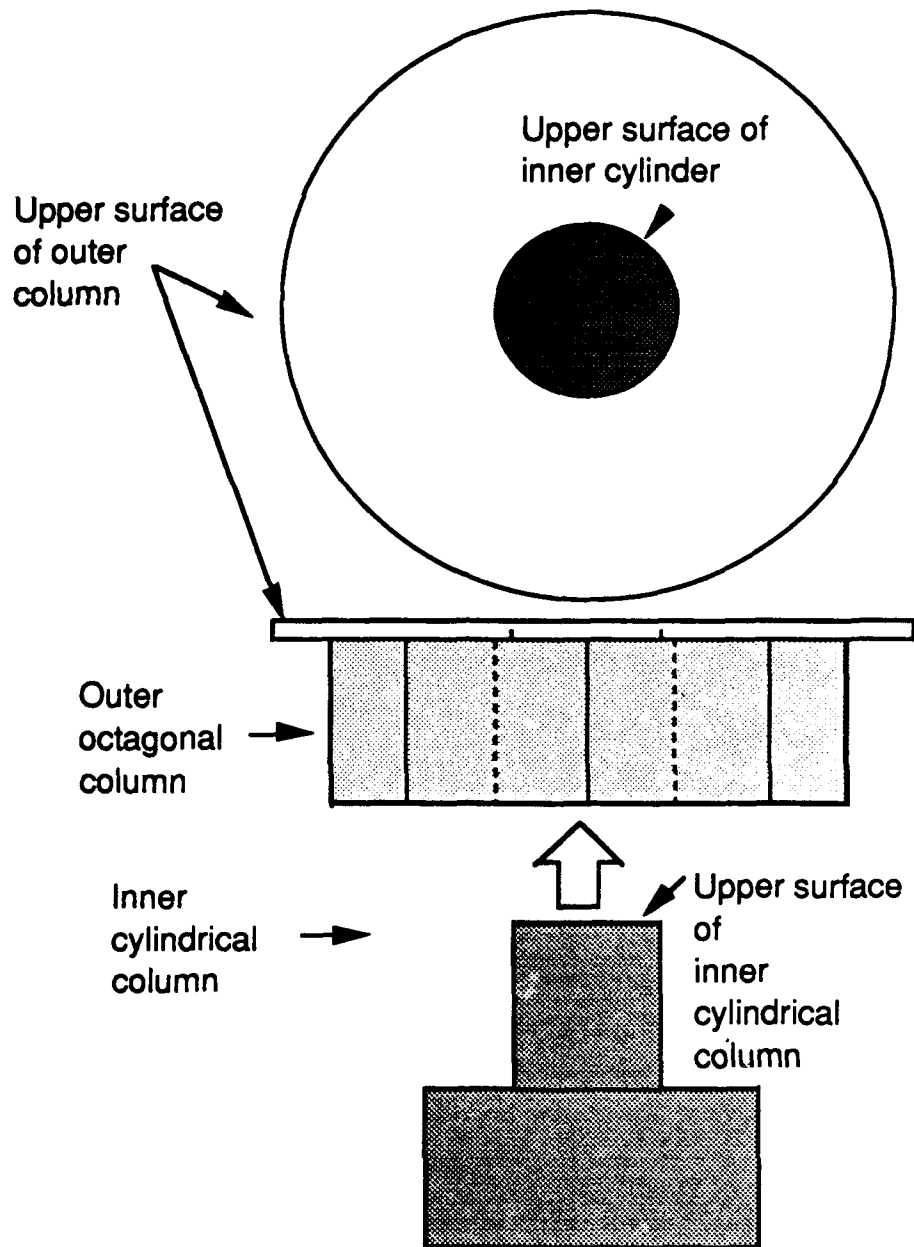


Figure 6. Schematic drawing of the Styrofoam column showing the component parts. The upper figure shows the mounting surface from the top, while the lower 2 figures present a sideview of the 2 parts of the column.

column (11.28 cm or 4.44 in. radius and 35.56 cm or 14 in. height) is attached coaxially. The upper surface area was approximately 400 cm² (62 in²) in area. The outer component of the Styrofoam platform consisted of an upper circular disk (25.22 cm or 9.93 in. radius and 2.54 cm, or 1 in., thick) attached to an octagonal base (each face approximately 16.51 cm or 6.5 in. wide). The outer component was hollowed out to a radius of approximately 11.43 cm (4.5 in.) for approximately 5.08 cm (2 in.) below the upper surface and to a radius of 12.7 cm (5 in.) for the remainder of the 35.56 cm (14 in.) height. This geometry provided for a total upper surface area of approximately 2,000 cm² (310 in²) whenever the outer (and detachable) component was used. By making the major portion of the inner hollow slightly greater in radius than the radius of the inner cylindrical component, the friction incurred in the removal of the outer component was greatly reduced. The snug fit at the upper 5.08 cm (2 in.) of the combined components provided all the support needed at the top to ensure a sturdy upper surface for specimen placement. The bottom of the octagonal portion of the outer Styrofoam component rested symmetrically upon approximately 81 cm² (12.56 in²) of the upper surface of the lower cylindrical portion of the inner Styrofoam component, thereby providing sufficient support for loading on the Styrofoam outer component. The bottom surface of the Styrofoam inner component was attached permanently with glue and protruding wooden dowels to the rotatable wooden circular disk of the elevator system (described later). The Styrofoam platform could then easily be rotated through 360°. The pedestal system is shown in Figures 7 and 8, and is schematically shown in Figure 9. The base of the system is 244.35 cm (96.2 in.) long with a 80.01 cm (31.5 in.) wide trough through which a large triangular wedge travels. The wedge has a 83.06 cm (32.7 in.) height, a 111.76 cm (44 in.) base, a 137.92 cm (54.3 in.) hypotenuse, and a 25.40 cm (10 in.) width. A smaller, triangular elevator platform rests atop the wedge such that the hypotenuses of the 2 structures abut. The elevator platform has a wooden cylindrical rod on each of the 2 outside surfaces which extends outward into vertical guide slots in the sidepanels of the base. Thus, when the wedge moves horizontally along the trough, it imparts a vertical motion to the elevator platform. Movement of the large triangle is controlled by a wooden push rod which extends horizontally from the front of the wedge and passes through a vertical support panel at the far forward part of the base. A wooden clamping mechanism there is used to brake the rod when the desired specimen elevation is achieved. The wedge approach to building an elevation system offered simplicity of construction and operation. Further, any future need for

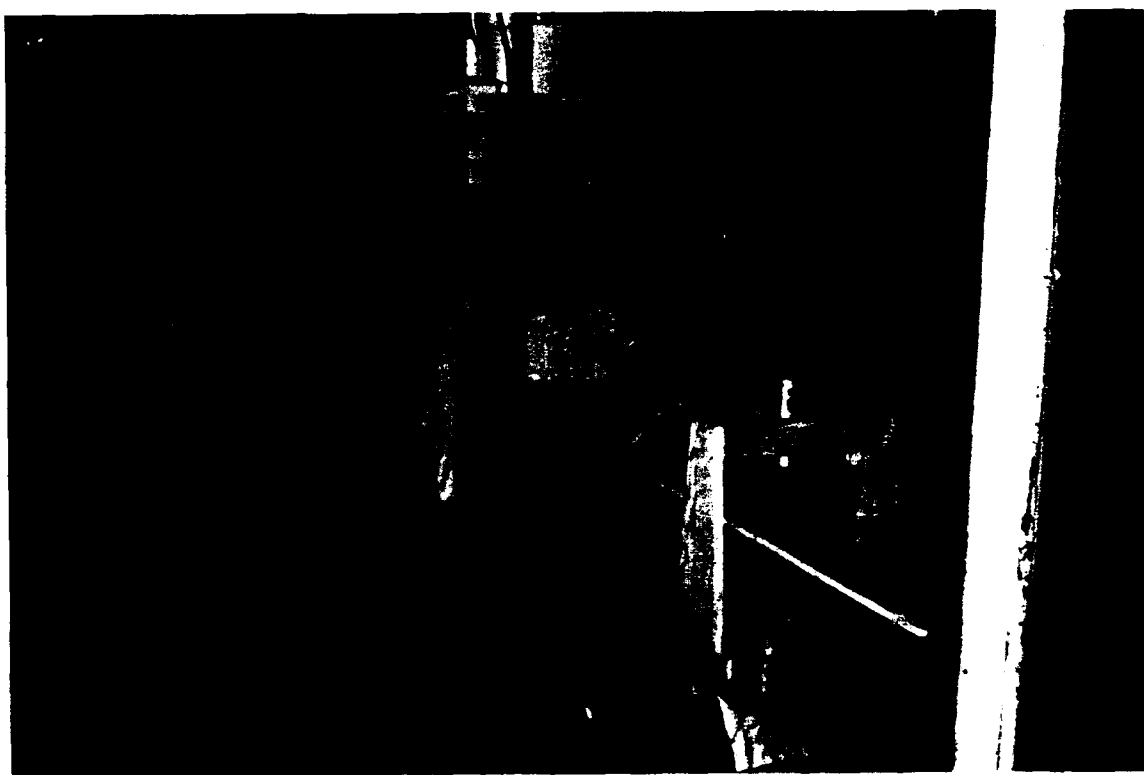


Figure 7. Pedestal system upon completion of construction at the Georgia Tech Machine Shop.

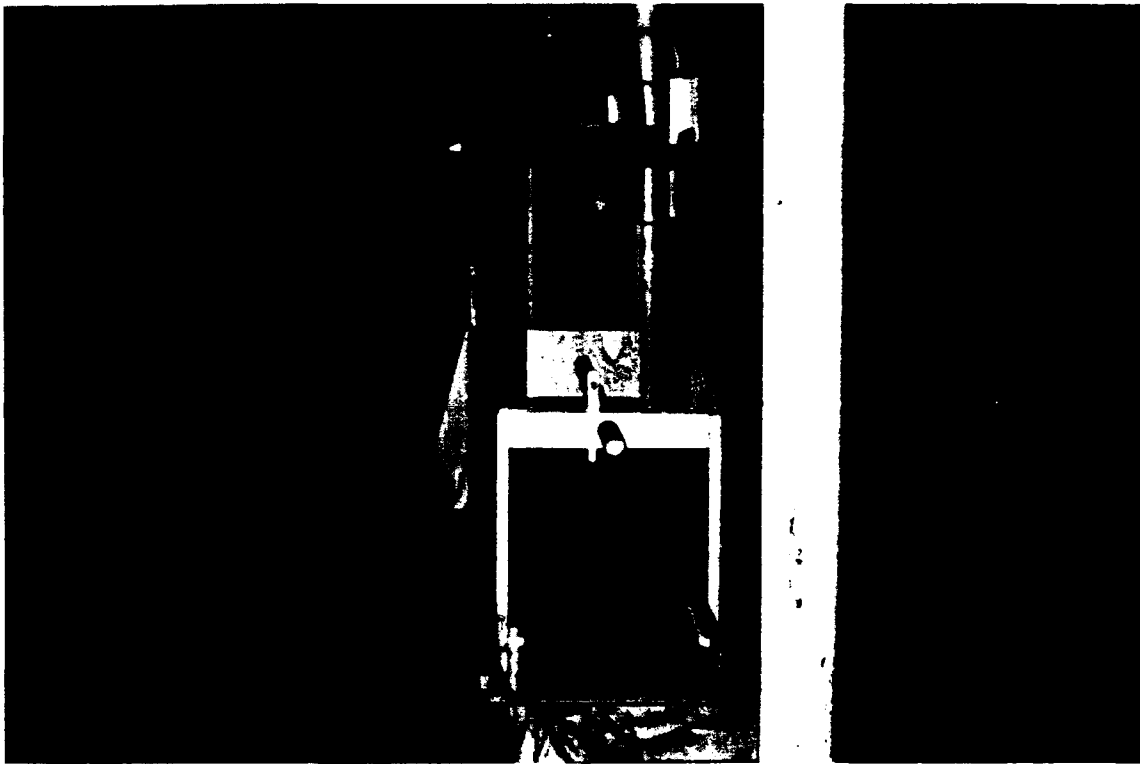


Figure 8. An end-view of the pedestal system upon completion of construction at the Georgia Tech Machine Shop.

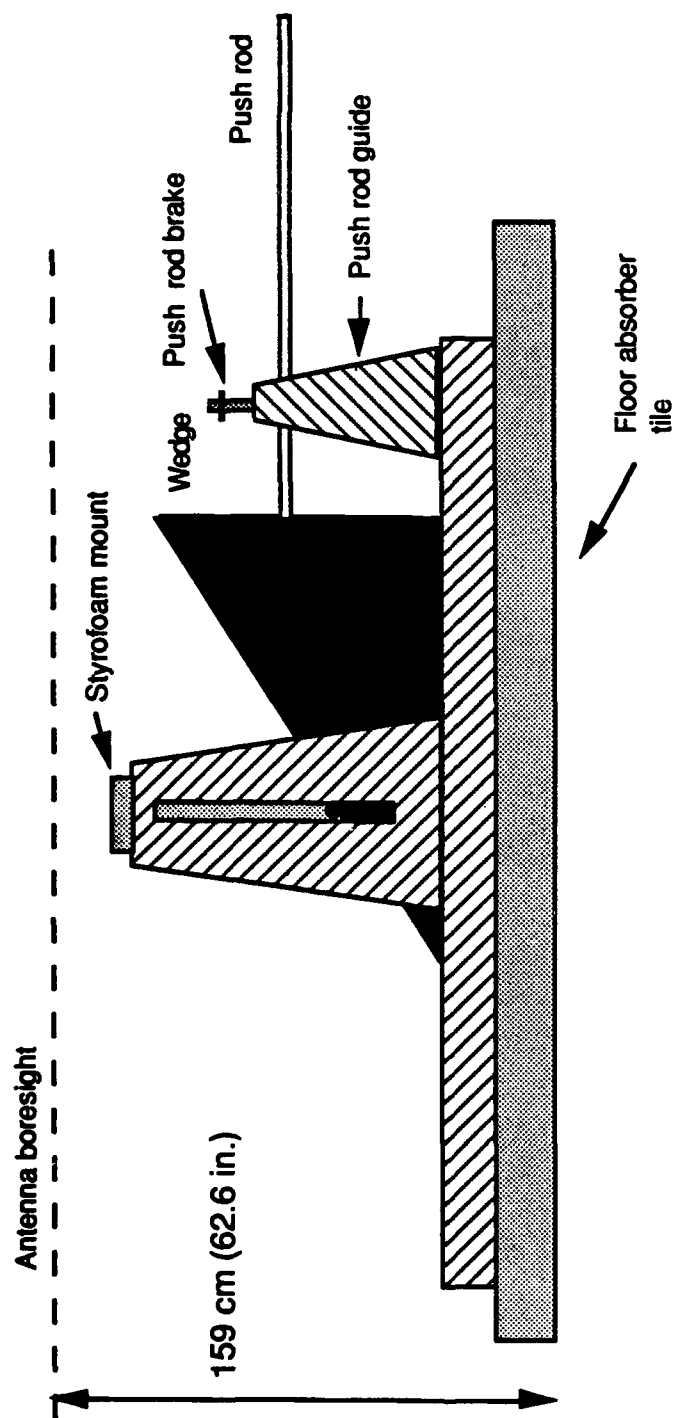


Figure 9. Schematic drawing of the pedestal system.

replacement of parts would be easy and inexpensive to meet. The ideal mechanical advantage of the wedge depended on the ratio of the length of the hypotenuse to the height. These dimensions were constrained by (1) the size of the anechoic chamber and, hence, the length of the base of the elevator system, and (2) the desire to keep the uppermost wooden parts of the pedestal system outside (below) the half-power beamwidth of either uncorrected (i.e., lensless) horn antenna. The latter measure would not only reduce any perturbing interaction between wood and the incident field during Gaussian lens operation of the horn antennas, but would also offer good performance should researchers desire to use it in experimentation with the uncorrected antennas. The ideal mechanical advantage of the wedge was calculated to be approximately 1.7 and frictional effects were reduced as much as possible with nylon strips. A 1.91 cm (0.75 in.) thick circular disk with a short cylindrical axle extending out from the center of one surface was mounted flush with the upper (horizontal) surface of the elevator platform by placing the axle into a hole in the elevator platform and capping it from underneath. Thus, the disk could be easily rotated 360° around the axle. The bottom surface of the Styrofoam platform was attached to the disk with glue applied directly to the interfacial surfaces as well as to wooden dowels inserted into both the disk and the Styrofoam.

Pedestal Performance

The pedestal was built and placed in the anechoic chamber at USAFSAM. The pedestal was light enough to be easily moved about in the chamber by one person, but heavy enough and long enough to provide a stable platform for specimen mounting during experimentation. The long axis of the base was aligned approximately along the perpendicular bisector of the line between the horn antenna apertures, and the vertical axis of the cylindrical Styrofoam platform was placed at the intersection of the 3 m (9.84 ft) points along boresights of the antennas. Thus, without moving the pedestal at all, it could serve either antenna by rotating the Styrofoam platform. Additionally, the Styrofoam platform could be rotated for a particular antenna to present different polarization geometries without the researcher actually touching the specimen. With this arrangement of the pedestal, the wooden push rod used for moving the wedge extended toward the plane of the antennas and

extended partially beneath the lens mounting table (see Fig. 3) during the lowest elevation of the specimen.

OPEN-WAVEGUIDE FIELD PROBES

Design Concepts and Components

The open waveguide field probes were constructed of straight waveguide sections attached to thermistor mounts with flange screws. The straight waveguide sections supplied by Hughes were 17.78 cm (7 in.) long with round flanges on each end. One flange of each section was machined off and the exposed rectangular cross section smoothed to produce a field-sensing aperture. The other end of each section, with the flange intact, was mated to the appropriate thermistor flange with 4 flange screws. Removal of a flange left approximately 17.14 cm (6.75 in.) of total length to the waveguide section, of which 16.51 cm (6.50 in.) (i.e., minus the length of the remaining flange) was the rectangular waveguide portion. This length was equivalent to 19.26 wavelengths for the 35 GHz waveguide and 52.00 wavelengths for the 94.5-GHz waveguide. These lengths permitted adequate damping of fields on the waveguides which might travel to the flanges, be reflected, and return to the aperture. For the 35-GHz probe assembly, a Hughes 45771H Ka-band thermistor mount and 45431H Ka-band straight waveguide section with round flanges were used and for the 94.5 GHz probe, a Hughes 45776H W-band thermistor mount and 45436H W-band straight waveguide section with round flanges were used. Flange attachments were made with Hughes 45550H waveguide flange screws. Hewlett-Packard 8120-1359 cable (15.24 m or 50 ft.) was used to route the thermistor outputs through the anechoic chamber walls to a Hewlett-Packard 432B power meter in the adjacent instrumentation room.

For radiation pattern measurements, either probe could be mounted in a wooden arm which extended perpendicularly from the vertical axis of the positioner into the exposure volume. A circular hole just large enough in diameter to permit a snug fit for the 3.30 cm (1.3 in.) diameter thermistor mount was cut into the arm at the distal end. The probe was then aligned with antenna boresight by

establishing boresight visually, with either a Class II HeNe laser or with the arrangement of strings currently in place for that purpose, and then visually adjusting the probe until the lengthy waveguide section was parallel to boresight.

The physical aperture of the 35-GHz waveguide was 0.711 cm (0.28 in.) in width and 0.365 cm (0.14 in.) in height. Assuming a 50% aperture efficiency a 0.12-dB loss in the waveguide, then attempting field measurements at the anticipated maximum level of 1 W/cm² would theoretically present 126.5 mW of power to the thermistor mount. This power level would be greatly in excess of the 10 mW the mount is capable of handling; therefore, the power density used for field mapping at 35 GHz should be constrained to peak values no greater than approximately 30 mW/cm², since at even 100% efficiency, this density would produce a theoretical maximum power of 7.6 mW at the thermistor input. The aperture dimensions for the 94.5-GHz waveguide are 0.254 cm (0.1 in.) in width and 0.127 cm (0.32 in.) in height. Assuming a 50% aperture efficiency and waveguide losses of 0.47 dB, an incident power density of 1 W/cm² would produce 126.5 mW at the thermistor. Therefore, keeping the incident power density below 70 mW/cm² for field mapping purposes would appear safe. However, a "worst" case assumption of 100% aperture efficiency would suggest keeping the fields below approximately 300 mW/cm² at 94.5 GHz, and this would theoretically produce only 8.6 mW at the thermistor input. The safe recommendation would be to map at a power density no greater than 100 mW/cm², especially since this is the maximum value available with the Narda field monitors used to measure power densities in the chamber at this time.

Probe Performance

During the September 1990 site visit to USAFSAM, the 35-GHz probe was tested in the anechoic chamber without using the lens. A calibrated Narda field monitor was placed on the pedestal and aligned with the 35-GHz corrugated conical horn boresight at 3 m (9.94 ft) from the antenna aperture. Power density measurements were then made for 6 different power settings of the transmitter. The Narda was then removed and the probe substituted, with the aperture at the 3 m (9.84 ft) point along boresight. A cone of Emerson & Cuming AN 72 sheet absorber was wrapped around the

probe so just the tip of the probe was exposed at the apex of the cone. The cone lateral surface flared rearward to cover the portion of the probe from the tip to the middle of the thermistor mount, thereby shielding the remainder of the probe from the field line-of-sight. The transmitter was then stepped through the same sequence of power settings as with the Narda power density meter and the outputs of the probe observed with a HP 432B power meter. An additional section of sheet absorber was then placed over the remainder of the open-waveguide field probe and the test repeated. Data from this set of experiments are given in Table 3. Figure 10 is plot of the HP 432B power meter (in mW) vs. the transmitter settings (in mW) which shows a very linear relationship between the two. Figure 11 is a plot of the HP power meter output vs. the Narda power density meter measurements (in mW/cm²) at 35 GHz for the same transmitter settings, which are given in parentheses adjacent to the data points in the figure. The transmitter appears to produce a power density which is linear with the power settings at least up to the 100 mW/cm² limit of the Narda. The linear relationship between the probe and both the Narda output and the transmitter power settings indicate that it can be calibrated to provide accurate and reliable power density measurements throughout the exposure volume, at least up to those levels of power density which produce the maximum safe power level of 10 mW at the input of the thermistor as discussed earlier. Additionally, we can note from Table 3 that the extra sheet of absorber placed on the probe had negligible influence on the probe response, at least with regard to the relative measurements pertinent to pattern mapping.

The 94.5-GHz probe was not tested during the site visit because of time limitations. However, the probe can be expected to operate equally as well as the 35-GHz probe for radiation pattern mapping. This probe, too, should be wrapped with sheet absorber in the shape of a cone as in the case of the 35-GHz probe.

Figure 12 is a close-up photograph of the 35-GHz probe positioned over the Styrofoam surface by the positioner system. The waveguide, thermistor mount, wooden positioner arm, and the output cable of the thermistor mount can be observed; however, the sheet absorber cones used for attenuating reflections of millimeter-wave energy from the probes are not shown in this figure.

**TABLE 3. MEASUREMENT DATA FROM THE 35-GHZ OPEN-WAVEGUIDE
FIELD PROBE TEST**

Transmitter Setting (mW)	Narda Monitor (mW/cm²)	35-GHz Probe^a (mW)	35-GHz Probe^b (mW)
2.00	4.3	1.83	1.81
2.50	5.5	2.29	2.26
3.00	6.6	2.74	2.71
3.50	7.7	3.19	3.17
4.00	8.8	3.65	3.62
4.50	10.0	4.11	4.08

^aSheet of absorber wrapped around waveguide section only.

^bAbsorber wrapped around both waveguide section and thermistor mount.

REMOTE-CONTROLLED POSITIONER

Design Concepts

This phase of the project undertook the design and construction of a remote-controlled positioning system. This positioning system was to be capable of positioning a millimeter-wave field probe within a 1 m (3.28 ft) X 0.5 m (1.64 ft) X 0.5 m (1.64 ft) volume. The system was also to be capable of feeding back to a remote computer the position of the thermistor. The drive mechanisms for the system were to be controlled by the remote computer. Since the thermistor would frequently be within the high power cone of the millimeter-wave field, a method of supporting the probe was to be devised that would minimize the use of reflective materials around the thermistor. The design allowed for simple construction and maintenance as well as for an easily implementable servo feedback loop for control. All the axes were identical in design and function which allowed for the use of common components in assembly and replacement. The design incorporated as many off-the-shelf components as possible to allow for easy interchange or replacement. Only the structure was custom built for this design.

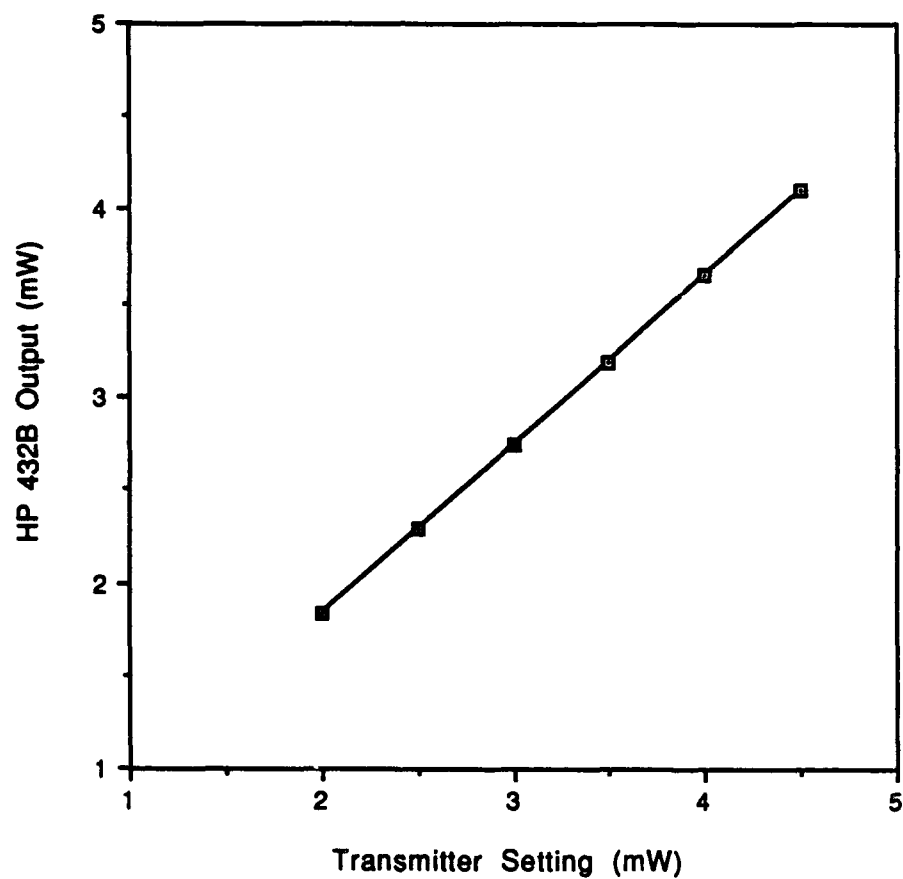


Figure 10. Plot of the HP 432B Power Meter output vs. the transmitter setting.

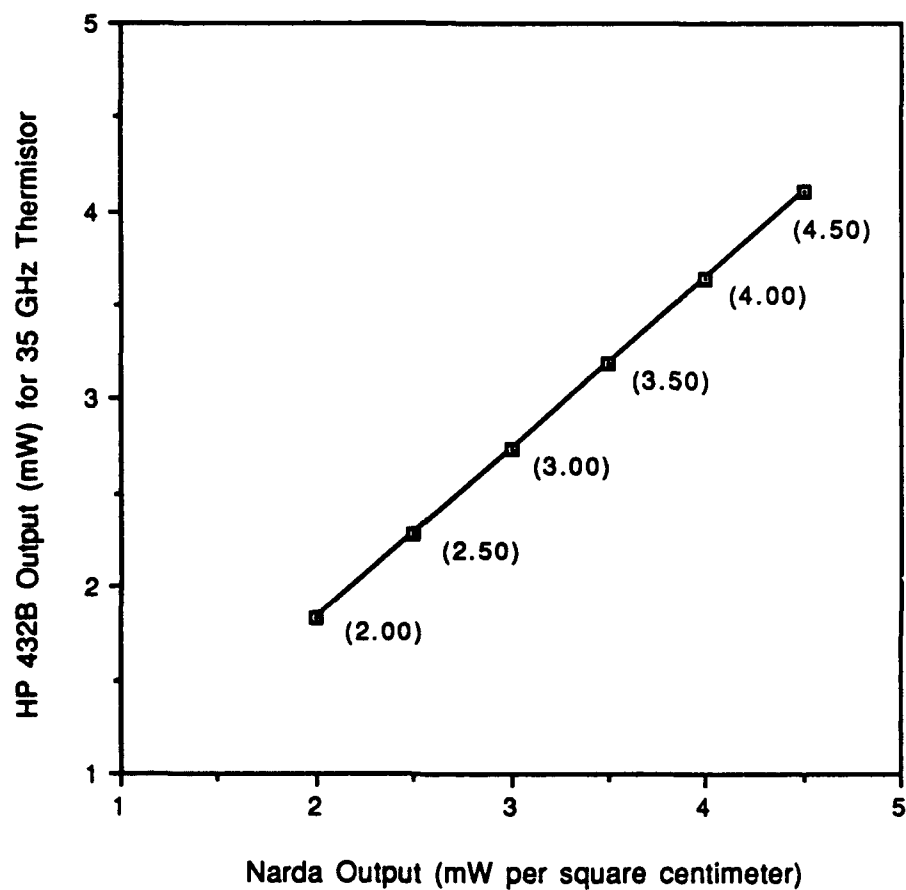


Figure 11. Plot of the HP 432B output vs. Narda field probe at 35 GHz. Transmitter settings (mW) are given in the parentheses.

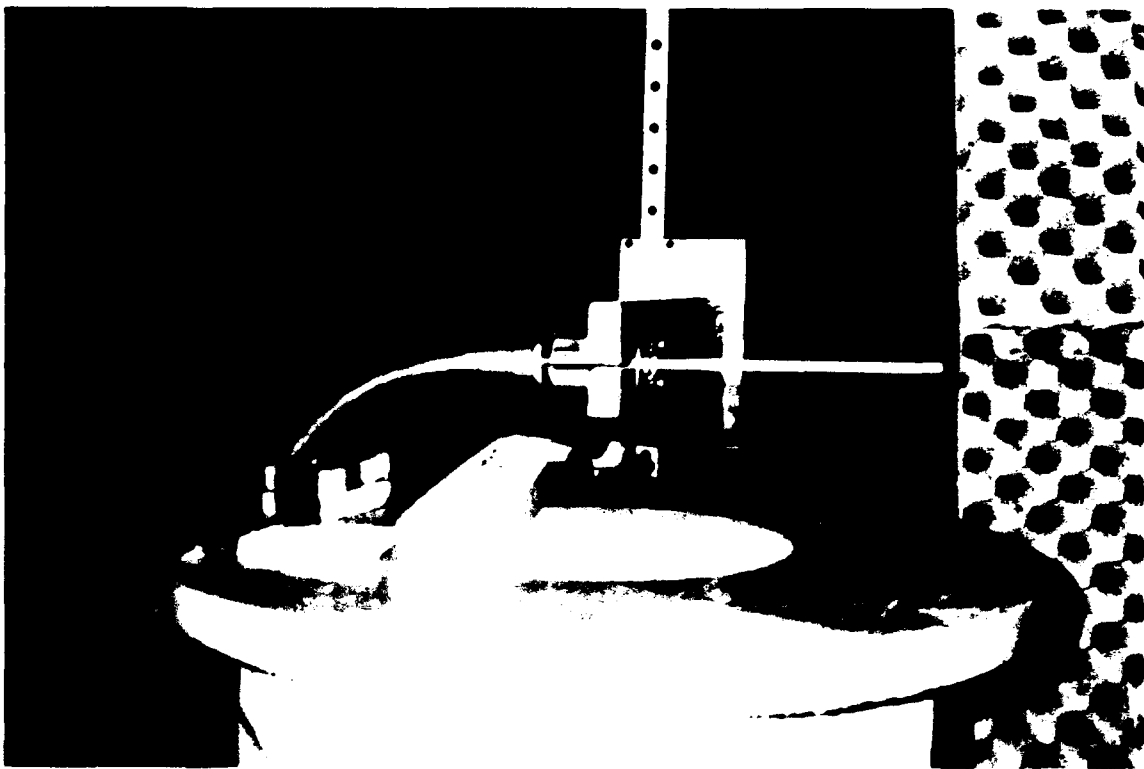


Figure 12. Close-up of the 35 GHz probe showing the waveguide, thermistor mount, wooden positioner arm, and the output cable.

Positioner System Components

Components used in this system were chosen for their strength, stability, and repeatability. The design consisted of a carriage covering a 3-axis cartesian coordinate system; X- (along boresight), Y- (transverse horizontal to boresight), and Z- (transverse vertical to boresight) axes. The system allowed a range of travel of 100 cm (39.37 in.) in X, 50 cm (19.69 in.) in Y, and 50 cm (19.69 in.) in Z with continuous positioning throughout these ranges. The motion was accomplished using a 5 mm (0.20 in.) pitch lead screw with 1.27 cm (0.5 in.) double linear rails for stability. Most linear motion products available commercially exceeded the required specifications for this system so cost was the driving factor for the choices made. The following is a summary of design considerations.

Configuration: A 3 degrees-of-freedom platform was specified to map out the millimeter-wave field above the specimen platform within the millimeter-wave chamber. The system had to be able to move a millimeter-wave thermistor mount around within the described volume with the least amount of *interference and reflection*. For this reason, the positioner's metallic parts were designed such that they never intruded into the exposure volume. The only component of the positioner system to extend into the exposure volume was a wooden arm which was attached to the vertical rail at one end and held the open-waveguide field probe at the other end.

Speed: Speed was not a major concern since this system was to be used for dosimetry and mapping only. However, care was taken to control the acceleration and deceleration to minimize overshoot and swinging of the wooden arm.

Payload: The positioner needed to carry only the weight of the platform itself and the wooden arm with the probe in place. The probe (thermistor and waveguide) weighed less than 0.23 kg (0.5 lbs) and the wooden arm weighed approximately 1.13 kg (2.5 lbs). All of the linear motion components used were capable of carrying loads of up to 90.60 kg (200 lbs). Since all of the structure was aluminum, the capacity of these components far exceeded the loads met.

Accuracy: Position feedback sensors needed to be of high resolution and accuracy for precise mapping of the field. Since continuous feedback was required, highly linear, accurate potentiometers were used for position sensing. All feedback was achieved mechanically through anti-backlash gears to minimize backlash and error. The actual resolution of the feedback system was determined by the analog-to-digital (A/D) converter used. Since the potentiometers offered continuous feedback throughout the full range of motion, the A/D converter determined the accuracy according to the number of bits it used for digital encoding.

Modularity: The system needed to be easily reconfigurable for a different range of motion and portable so that it could be used in other chambers on the site. Were a smaller system desired for a different application, this system could still be used by constraining the length of travel on each axis. Were a larger system desired, the design could be extended to the lengths needed for the application.

Reliability and Repeatability: The positioner system needed to possess a high degree of repeatability and reliability. These features can be described as capabilities for continuous operation at nominal speed and accuracy with no degradation in performance over time aside from that incurred through normal wear of the components.

Mechanical Design

The final configuration for the positioning system is shown in Figures 13 and 14. This configuration allowed the probe to cover a volume that was 100 cm (39.37 in.) X 50 cm (19.69 in.) X 50 cm (19.69 in.) above the specimen platform. The design also minimized the exposure of the structure to the field, and thereby minimized reflections and interference. The wooden arm that extended into the field was nearly millimeter-wave transparent. The slit leading from the end of the wooden arm to the thermistor-clamping hole near the end of the arm facilitated the interchange of the 2 different thermistors and their alignment.

Structural design of the positioner was simple and lightweight. Each axis had an aluminum base that was used to support the linear rails and motors. Each axis also had a precisely machined set of bulkheads at each end that held the motor and feedback mechanisms. Figure 15 shows the potentiometer and gear arrangement for the feedback. As can be seen in the figure, anti-backlash gears were used between the ball screw and the potentiometer to minimize backlash and position errors. Steel was used for the construction of the tower for the Z-axis. The use of steel was done for stability and ease of construction, since the metal was easy to bend into the configuration needed.

The motors used were 6 W DC motors with graphite brushes. The rated nominal input voltage for these motors was 18 V with maximum continuous current being 575 mA. The rated no-load speed was 7,750 rpm which translated to a maximum linear speed at each axis of 34.4 mm/s (1.35 in./s). The motors were mated to a 2 stage planetary gearhead with a 18.75:1 gear reduction. The position feedback potentiometers were 20-turn, 1 k Ω potentiometers with linearity of $\pm 0.5\%$ through full range of motion. The system was set up for a range of -10 V to +10 V for the feedback. The A/D converter chosen will determine the resolution of the system: the greater the number of bits used to accomplish the encoding, the greater will be the resolution throughout the range of motion.

Positioner Performance

The system was constructed and installed at USAFSAM in September 1990. All components of the system were tested after installation and performed as designed. The 3 axes were tested individually by using a variable power supply connected to the motors. Each motor was driven through the full length of travel several times to ensure workability. The potentiometers were calibrated so that, when the axis being controlled was in the middle of travel, the corresponding potentiometer was centered. Again, the system was operated with the variable power supply while the feedback from the potentiometers was monitored and this proved successful as well. Instructions were given on how to connect the system to a computer for controlled mapping of the fields.

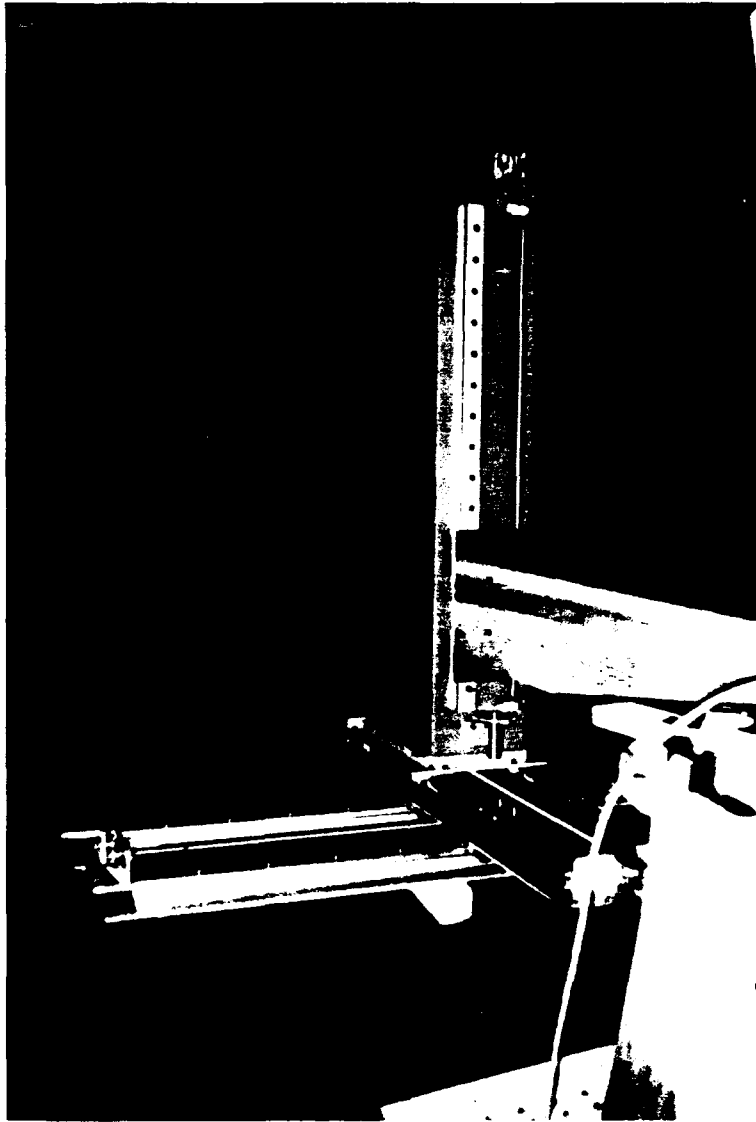


Figure 13. The 3-axis positioning system from the front showing all 3 rails and the wooden arm extending from the vertical rail out over the pedestal.



Figure 14. The 3-axis positioner system from the rear looking out over the pedestal system.



Figure 15. The 3-axis positioner system showing the potentiometer and gear arrangement for positioning feedback.

REFERENCES

1. Clarricoats P.J.B., and P.K. Saha. Radiation Pattern of a Lens-Corrected Conical Scalar Horn. *Electron Lett* 5:592-593 (1969).
2. Kildal, P.S., K. Jacobsen, and K.S. Rao. Meniscus-Lens-Corrected Corrugated Horn: a Compact Feed for a Cassegrain Antenna. *IEE Proc* 131:390-394 (1984).
3. Goldsmith, P.F., T. Itoh, and K.D. Stephan. Quasi-Optical Techniques. In: K. Chang (ed.), Handbook Of Microwave and Optical Components Vol I, pp. 344-363. New York: John Wiley & Sons, 1989 .
4. McEwan, N.J., and P.F. Goldsmith. Gaussian Beam Techniques for Illuminating Reflector Antennas. *IEEE Trans Antennas and Propagat* 37:297-304 (1989).
5. Goldsmith, P.F. Quasi-Optical Techniques at Millimeter and Submillimeter Wavelengths. In: K.J. Button (ed.), Infrared and Millimeter Waves, 6:272-343. New York: Academic Press, (1982).
6. Wylde, R.J. Millimetre-Wave Gaussian Beam-Mode Optics and Corrugated Feed Horns. *IEE Proc* 131(Pt. H):258-262 (1988).
7. Antenna Handbook, Chapt 8 (eds.: Y.T. Lo and S.W. Lee). New York: VanNostrand Reinhold Co., (1988).
8. McMillan, R.W., et al. Near Millimeter Wave Radar Technology. Interim Technical Report (Vol I), U.S. Army Contract DAA70-C-0108, Oct. 1982.
9. Simonis, G.J., et al. Characterization of Near-Millimeter Wave Materials by Means of Non Dispersive Fourier Transform Spectroscopy. *Int J Infrared and Millimeter Waves* 5:57-73 (1984).
10. Clarke, J.A. and R.J. Dewey. Millimeter Wave Imaging Lens Antenna. *Int J Infrared and Millimeter Waves* 5:91-101 (1984).
11. Bhartia, P. and I.J. Bahl. Millimeter Wave Engineering and Applications. New York: John Wiley & Sons, 1984.

APPENDIX
PHOTOGRAPHS OF
MACHINED SURFACES



Figure A-1. Basic cylindrical block of Rexolite to be machined in to the biconvex 35-GHz dielectric lens. Only one surface has been prepared for contouring at this point.

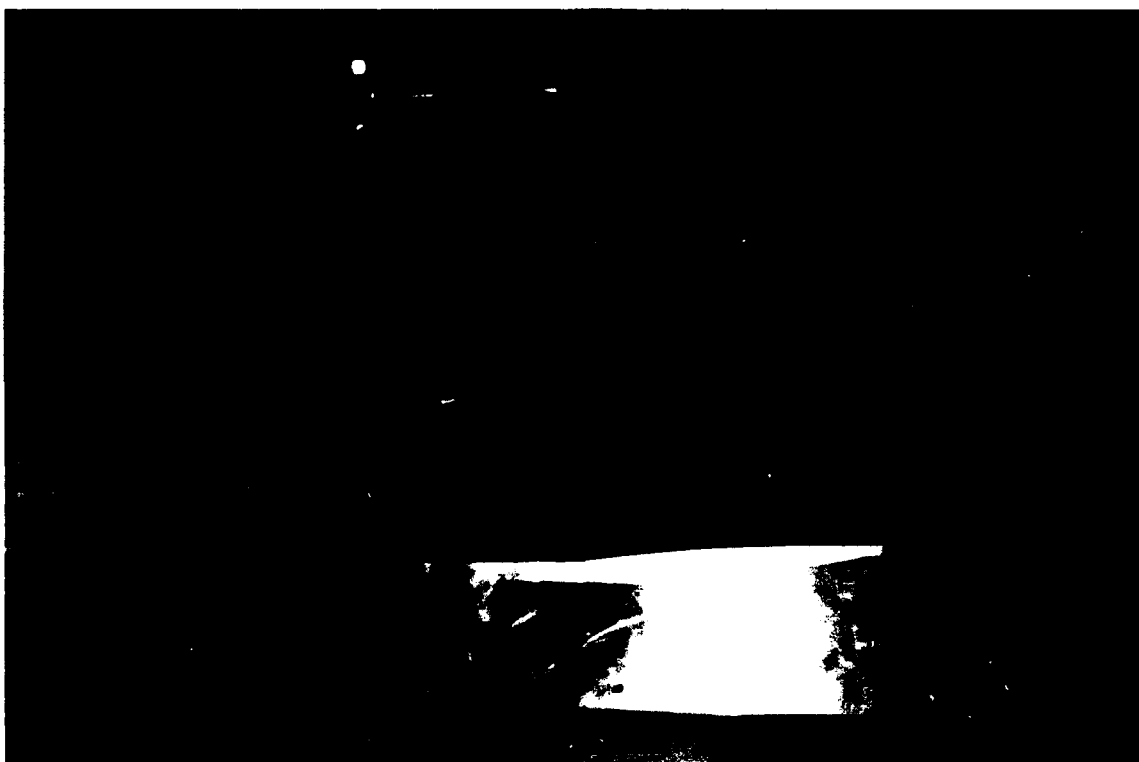


Figure A-2. Another view of the Rexolite block of Figure A-1 following surface contouring. The metal templates used to control the machinings of the two 35-GHz lens surfaces are shown.



Figure A-3. Machining of one of the 35-GHz lens surfaces.



Figure A-4. Completed contouring of the lens surface.

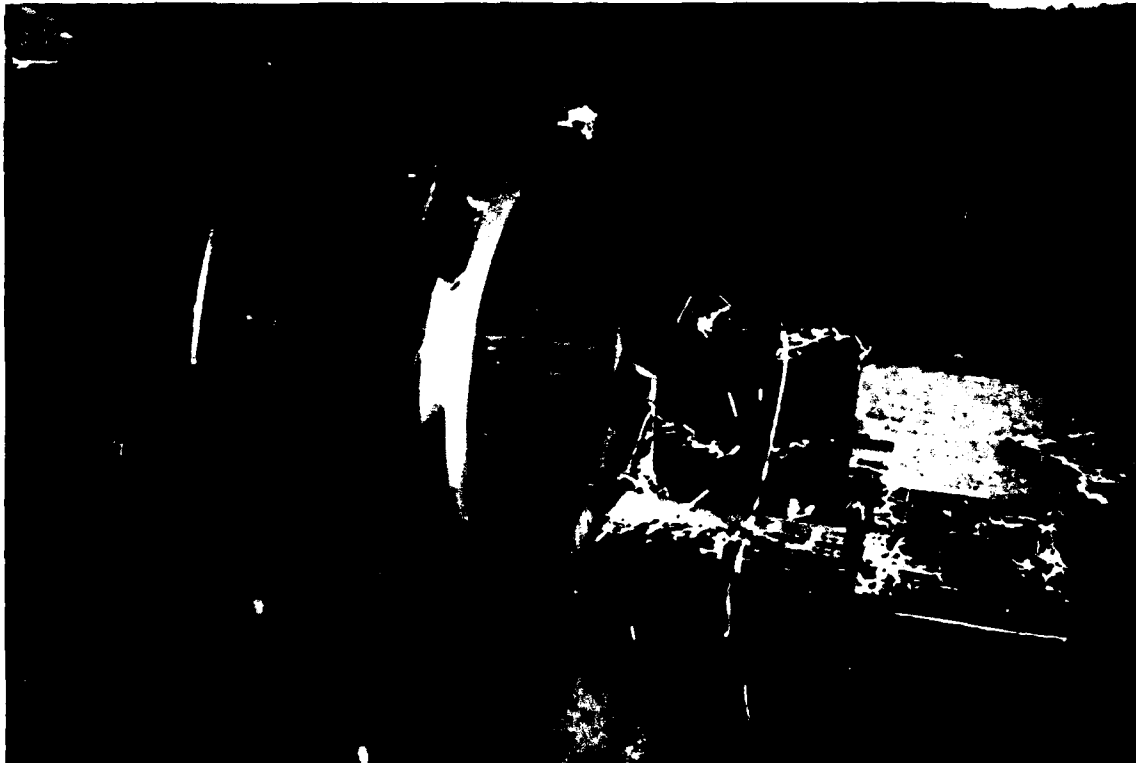


Figure A-5. Another view of the lens surface of Figure A-4. Note the discarded Rexolite.

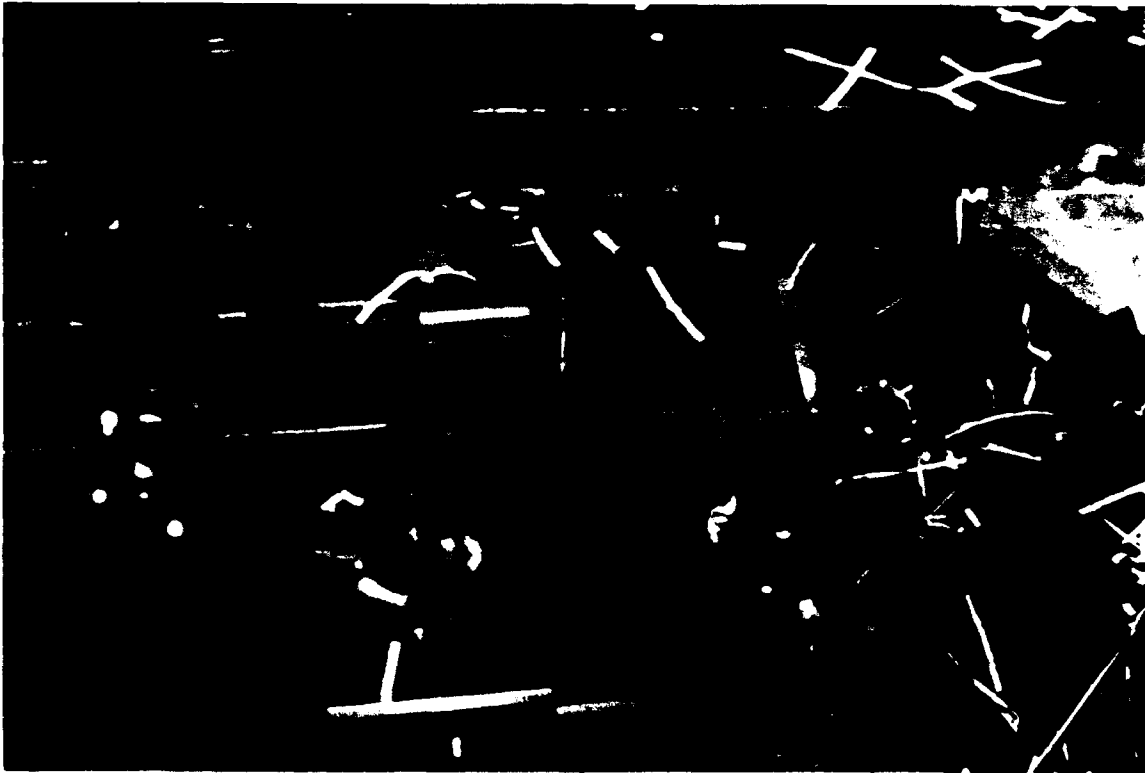


Figure A-6. Template being used to control surface contouring during the machining of the lens shown in Figures A-4 and A-5.

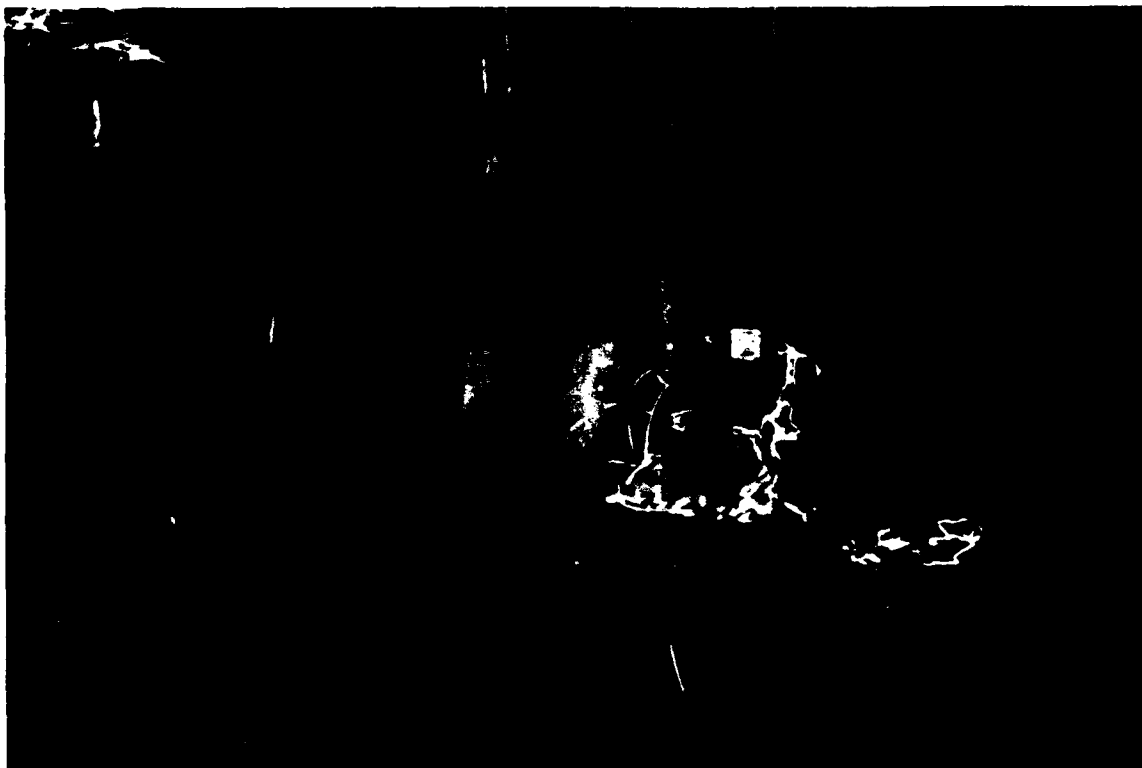


Figure A-7. Grooving of one of the 35-GHz dielectric lens surfaces.

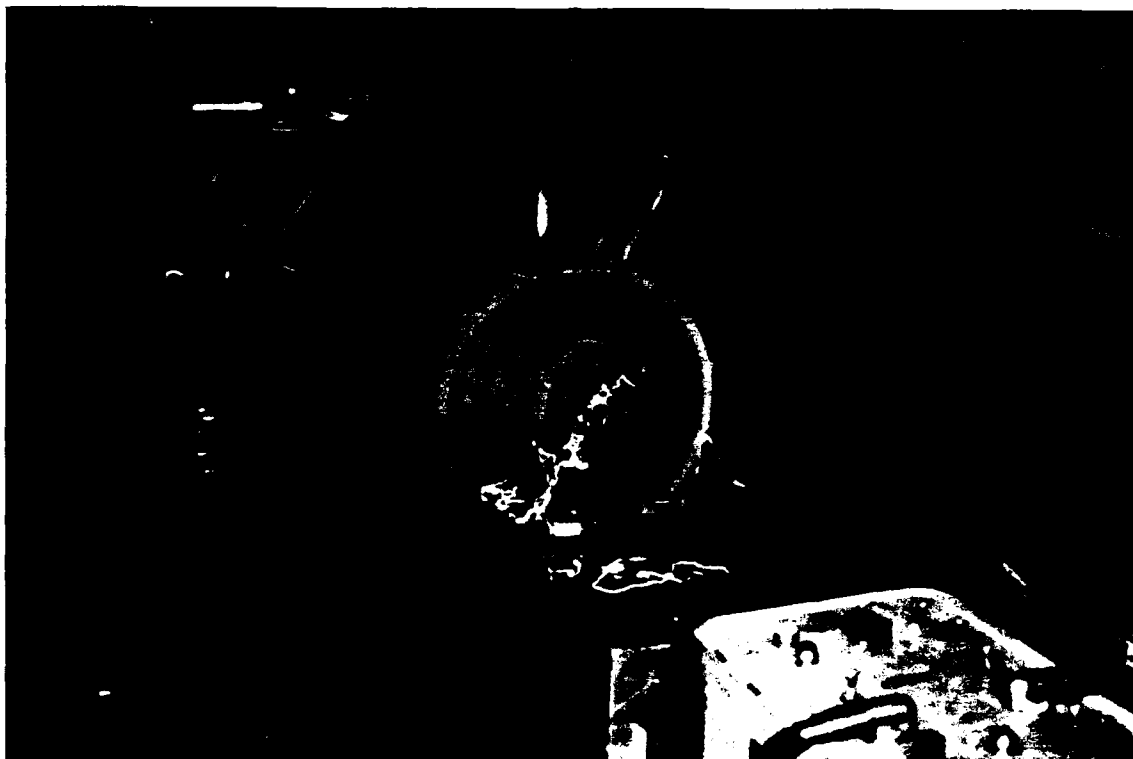


Figure A-8. Another view of the surface grooving process of Figure A-7. Note the "threads" of Rexolite being thrown off to the upper right region of the photograph by the lathe.



Figure A-9. Finished 35-GHz lens clearly showing the grooving.